Yang, J.; Blawert, C.; Lamaka, S.V.; Snihirova, D.; Lu, X.; Di, S.; Zheludkevich, M.L.:
Corrosion protection properties of inhibitor containing hybrid PEO-epoxy coating on magnesium.
In: Corrosion Science. Vol. 140 (2018) 99 - 110.
First published online by Elsevier: 15.06.2018

DOI: 10.1016/j.corsci.2018.06.014
https://dx.doi.org/10.1016/j.corsci.2018.06.014

Corrosion protection properties of inhibitor containing hybrid PEO-epoxy coating on magnesium

Junjie YANG[a, b], Carsten Blawert[b], Sviatlana V. Lamaka[b], Darya Snihirova[b], Xiaopeng LU[b,c], Shichun DI[a], Mikhail L. Zheludkevich[b,d*]*

a) School of Mechatronics Engineering, Harbin Institute of Technology, West Dazhi Road 92, 150001 Harbin, P.R China

b) Magnesium Innovation Centre (MagIC), Helmholtz-Zentrum Geesthacht, 21502 Geesthacht, Germany

c) Corrosion and Protection Division, Shenyang National Laboratory for Materials Science, Northeastern University, 3-11 Wenhua Road, Shenyang 110819, P.R China

d) Faculty of Engineering, University of Kiel, Kaiserstrasse 2, 24143 Kiel, Germany

Highlights

- A hybrid coating with duplex-layered structure was developed on magnesium
- The hybrid coating contains effective corrosion inhibitor of 3-methylsalicylate
- The corrosion performance of hybrid coatings was studied by EIS
- Active corrosion protection mechanism by inhibitor was characterized by SVET

Abstract

A hybrid PEO-epoxy coating was developed for magnesium. A highly-efficient corrosion inhibitor (3-methysalicylate) was impregnated into the anodized layer, which was sealed by an epoxy layer through dip-coating process. Influence of dip-coating parameters on coating properties was investigated. The corrosion performance was evaluated through general and localized electrochemical techniques. As a result, the epoxy layers registered superior resistance, whereas the anodized layer suppressed corrosion expansion. Longer immersion and triple-dipping favored the production of better sealed epoxy layer. The active protection mechanism was achieved by suppression the re-deposition of detrimental impurity and/or adsorption upon the exposed surface from incorporated inhibitor.

Key words: Magnesium; Hybrid coating; Corrosion inhibitor; SVET; Active corrosion protection;

1. Introduction

Up to date, plasma electrolytic oxidation (PEO) (also denoted as micro arc oxidation, MAO) has been widely accepted and practically applied for protecting Mg, Al, Ti and their alloys with aims of enhancing their corrosion performance and widening their applications in industry [1-4]. During PEO treatment,

constant short-living discharges occur on the sample surface, which result in the breakdown of the previously formed layers and partially fusion of substrate and coating materials [5]. It is well known that the thickness, morphology and composition of PEO coatings are fundamentally determined by the ingredients of electrolyte [6] and power regime [7]. Accordingly, considerable strategies regarding the optimization of these factors have been proposed for improving the corrosion performance of PEO coatings through increasing the thickness and compactness or changing their composition [8]. Indeed, a solid promotion in coating properties has been achieved by controlling these most basic parameters involved in PEO treatment. However, complete elimination of the micro pores and defects during PEO treatment is still impracticable due to its discharge assisted growth mechanism [9, 10]. Therefore, PEO coated samples still remain vulnerable to corrosion attack especially at the local defective areas because of the persistence of micro pores and defects in the coatings.

Nevertheless, the high plasma-assisted discharge temperature (*ca.* 1843–2370 °C [11]), porous and rough microstructure and physically/chemically stable properties of PEO coatings still provide them substantial opportunity to integrate with other surface treatment techniques for further improving their corrosion performance [4]. These potential techniques include in-situ particles addition in PEO electrolyte [12-14], chemical conversion [10, 15, 16], electrophoretic deposition [17], hydrothermal treatment [18], chemical vapor deposition (CVD) [19] and Sol-Gel [20-26]. Most of the given methods increased the corrosion resistance of PEO coatings through physically eliminating or sealing the pores and defects on the surface. On the other hand, the characteristic microstructure on PEO coatings has a great potential to serve as micro/nano reservoirs to store or carry corrosion inhibitive chemicals (termed as inhibitor here and after), which endow active protective capability to PEO coatings. For instance, inorganic ions (*e.g.* Ce^{3+} and PO_4^{3-} [14, 26, 27]) were in-situ or post-incorporated into PEO coatings as corrosion inhibitive species for reducing the degradation rate of PEO coatings. However, given that Ce^{3+} barely regarded as inhibitive species towards Mg corrosion [28], it suggests the inhibition action may be induced by the accompanied anions (*e.g.* PO_4^{3-} and NO_3^-) or improvement of coating compactness/thickness resulting from the incorporation of particles during PEO treatment. Later, as the development of organic corrosion inhibitors for Mg alloys [29-37], some highly-efficient compounds were successfully grafted into PEO coatings with imparting so-called "self-healing" ability to PEO-coated metals. As reported by Gnedenkov *et.al* [38, 39], the barrier (low frequency response at ~10^{-1} Hz in Bode plots) corrosion resistance of 8-hydroxyquinoline (8-HQ) loaded PEO coatings was one order of magnitude higher than the blank PEO sample without inhibitor addition and this difference was even enlarged after the polarization of both samples. More importantly, the active inhibitive action caused by 8-HQ was further confirmed by the localized scanning electrochemical techniques (SVET and SIET) results, when corrosion occurred within the artificial defect. Unfortunately, similar research is rather limited for Mg alloys, which may be ascribed to the lack of efficient inhibitors and understanding of the inhibition mechanisms.

Most recently, a comprehensive screening of corrosion inhibitors for Mg was conducted by Lamaka *et.al* [28], and several compounds were proven of efficiency in decreasing the corrosion rate of most commercial Mg alloys (*i.e.* WE43, ZE41, E21, AZ31, AZ91 and AM50) and pure Mg containing different levels of Fe impurity (*i.e.* CP-Mg-220ppm Fe, CP-Mg-50ppm Fe and CP-Mg-51ppm Fe). The critical principle of inhibitor selection was based on the capability of compounds to form stable complex with Fe^{2+}/Fe^{3+}, which suppressed the re-deposition of Fe on Mg surface that catalyzes the corrosion reaction within the corrosion cell [40]. Such an inhibition concept for Mg alloys is distinct from the adsorption (most organic inhibitors) and precipitate formation inhibition mechanism (most inorganic inhibitors and limited number of organic inhibitors *e.g.* 8-hydroxyquinoline [29]) reported in reference. Among the verified inhibitors, the derivatives of salicylic acid showed extraordinary high corrosion inhibition efficiency for most of examined materials due to their significant Fe complex ability.

In our present study, one of derivatives of salicylic acid (sodium salt of 3-methylsalicylate [28]) was impregnated into porous PEO coating, which is further sealed by a polymer layer to avoid unintentional loss of inhibitor in electrolyte. Epoxy-silane based agents were applied as the main components in the polymer for increasing the barrier property and adhesion strength of the outmost layer. In order to achieve the ideal corrosion performance of the hybrid PEO-epoxy coating, the influence of critical dip-coating parameters on the morphology and thickness of epoxy layers were investigated. The general corrosion characterization of the hybrid PEO-epoxy coatings was conducted in neutral (pH: 6.8-7.2) NaCl solution (3.5 wt.%) for one month employing Electrochemical Impedance Spectroscopy (EIS) method. To manifest the active corrosion protection capability caused by the inhibitor loaded in anodized layer, localized corrosion characterization technique, Scanning Vibrating Electrode Technique (SVET), was employed in monitoring the local current strength over the scratched samples in 0.05 M NaCl solution for 24 h.

2. Experimental

2.1. Materials

As-casted commercial pure magnesium (Mg) was used as the substrate material in present work. The chemical composition was determined by Spark OES (Spark analyser M9, Spectro Ametek, Germany) and the results are listed in Table 1. Rectangular specimens with dimension of 35 mm×35 mm×4 mm were used for HF pickling and PEO treatment. Prior to these treatments, specimens were ground with emery papers up to 1200 grit, then rinsed with deionized water and ethanol, and eventually dried in compressed air flow at room temperature.

2.2. Pre-treatments for Mg

Acid pickling and PEO treatments were employed as pre-treatments for fabricating oxidized layers on Mg surface. As the reference, bulk Mg specimens are etched in hydrofluoric acid (HF, 12 wt.%) for 15 min with building a uniform brownish layer on the surface. Magnesium fluoride (MgF_2) can be identified as the main composition of the conversion layer [41].

The PEO treatments for the samples were carried out in constant current mode with a fixed current density of 50 mA/cm^2 supplied by a pulse DC power source. The frequency and duty ratio were 200 Hz and 10%, respectively. During the treatment, Mg specimens and stainless steel tube were utilized as anode and cathode respectively. Basic alkaline solution containing KOH (2 g/L) and Na_3PO_4 (10 g/L) was used as the electrolyte. The electrolyte temperature was regulated within 20 ± 1 ℃ by a circulating cooling system and constant mechanical stirring. The PEO pretreatments lasted for 10 min, and then the samples were rinsed with distilled water.

Corrosion inhibitor, 3-methylsalicylic acid (3-MSA, $CH_3C_3H_6(OH)CO_2H$, Reagent Plus, 99%, Sigma-Aldrich Chemie GmbH, Germany), was dissolved in deionized water at a concentration of 0.05 M under constant magnetic stirring. Standard NaOH (1 M) solution was utilized for adjusting the pH of the solution until neutral level (pH: 6.8-7.2). Eventually, sodium 3-methylsalicylate solution was obtained. Metrohm 692 pH meter was used for monitoring the acidity during the preparation. For impregnating the dissolved inhibitor into the micro pores, PEO-coated specimens were immersed in 100 ml inhibitor-containing solution (0.05 M) in a well-sealed pressure container. A water pump was employed for constantly extracting the air from the enclosed volume (*i.e.* pores of PEO layers and air dissolved in deionized water). The incorporating process did not cease until no visible bubbles can be observed on the sample surface. After that, the inhibitor-loaded samples were dried in compressed air flow prior to epoxy sealing.

For verifying the incorporation of 3-MSA in PEO layers, one of the dried samples was fully immersed into 25 ml deionized water and then treated using supersonic for 5 min to promote the release of inhibitor from PEO layer. As follows, the sample was transferred to a new beaker containing the same volume (25 ml) of deionized water for repeating the procedure. The solutions obtained after soaking the inhibitor-loaded PEO sample was examined by UV-VIS spectrophotometer (UV-2550, SHIMADZU, Japan). The wavelength range and step incrementation was 400-200 nm and 0.2 nm, respectively. Fig. 1 shows the two derived spectra plotted in group with the standard liquid samples by dissolving 5×10^{-4}, 5×10^{-5} and 5×10^{-6} M of 3-MSA respectively. The concentrations of solutions treated by supersonic are found between 5×10^{-4} and 5×10^{-5} M, which confirm the storage of inhibitor within the anodized layer.

2.3. Synthesis and deposition of sealing agent

Hybrid PEO-epoxy coating was prepared similar to that described in [25]. However, considering low flash point of acetone, this solvent was replaced by dimethyl sulfoxide (DMSO) in epoxy-silane formulation. All chemicals and solvents used in current synthesis were purchased from Sigma-Aldrich Chemie GmbH, Germany. Three main ingredients compose the coating formulation: aminopropyltriethoxysilane (APTES), poly(bisphenol A-co-epichlorohydrin) glycidyl end-capped (PBA) and diethylenetriamine (DETA). The addition of APTES mainly contributes to the enhancement of bonding strength between epoxy and PEO layers whilst DETA serves as epoxy hardener. During the synthesis, APTES (**Beaker 1)** and DETA (**Beaker**

2) was dissolved in ethanol separately, whereas epoxy component, PBA, was dissolved in the mixture of ethanol and DMSO (volume ratio is 1:1, **Beaker 3**). After 1 h stirring, the silane (**Beaker 1**) and amine (**Beaker 2**) components were successively added into the epoxy solution (**Beaker 3**). The concentration of the solute components in the final formulation was 3 wt. % APTES, 35 wt. % epoxy and 4 wt. % DETA. The obtained final mixture was kept stirring for another 6 hours at room temperature prior to dip-coating process. A PC controlled dip coater (KSV NIMA, Finland) was utilized for performing the dip-coating for the etched and PEO coated specimens. All specimens fixed by the sample holder were placed vertically with respect to the level of solution, which facilitates the retreat of redundant solution from the sample. In order to investigate the influence of the critical dip-coating parameters (*i.e.* immersion and withdraw speed, dipping repetition and immersion period in epoxy formulation), different coating strategies were designed, as listed in Table 2. The interval between dipping repetitions was null, which indicated out of delay would occur when the specimen reached the upper limit position. The samples are nominated in the format of EE/PE-dipping repetition code (1-single dipping, 3-triple dipping) and immersion period code (S-5 s immersion, L-60 s immersion). For example, EE-3S denotes the Mg substrate etched with HF and covered with hybrid epoxy layer produced by three times dipping with 5 s delay in the epoxy formulation. After the dip-coating procedure, all coated samples were cured at 150 °C for 90 min in an oven with a fully open fan for sustaining a flowing air condition.

2.4. Characterization

All the EIS characterizations were performed in NaCl solution (3.5 wt.%) with a conventional three-electrode system (Gamry Reference 600). Coated Mg coupons were employed as the working electrode (exposed area was 1 cm^2), along with a platinum wire counter electrode and a saturated Ag/AgCl reference electrode. AC EIS measurements were carried out at open circuit potential (OCP) with respect to amplitude of 10 mV RMS sinusoidal perturbation over the frequency range from 10^5 to 10^{-2} Hz, and one-hour immersion was performed in the same solution before running the EIS measurement in order to achieve stable OCP values. The stabilized OCP values of coated samples immersed after 1 h, 24 h, 48 h and 168 h are listed in Table 3.

A scanning electron microscope (Tescan Vega3) equipped with an energy dispersive X-ray spectroscopy (EDS) was used for examining the surface and cross-section morphologies and chemical composition before and after corrosion. For observing the cross-sectional morphology, coated samples were cold mounted in resin and polished successively using 800, 1200, and 2500 grit emery papers followed by disc polishing employing colloidal silica 1 μm to mirror finish. A thin Au film was sputtered on the surface to avoid charging effect occurred upon electrically non-conductive materials.

Scanning vibrating electrode technique (SVET) was used to measure the local current density in the place of the artificial defects, which were intentionally scratched and drilled by a diamond tool with reaching the Mg substrate. The SVET detects the current density response via measurement of the potential variation caused

by ionic fluxes. A commercial SVET setup manufactured by Applicable Electronics and controlled by LV4 ASET software (Science Wares) was used. In brief, an insulated Pt-Ir microelectrode (Microprobes Inc.) was employed as vibrating electrode for SVET measurements. The diameter of the ball of platinum black was 15 ± 3 μm. The probe was placed 100 ± 5 μm above the sample surface, vibrating in the horizontal (X) and vertical (Z) planes relative to the surface with amplitudes of 17 μm. The vibration frequencies of the probe were 128 Hz (X) and 325 Hz (Z). Experiments were conducted during continuous immersion in 0.05 M NaCl solution, all the SVET measurements were conducted in a Faraday cage at room temperature.

3. Results

3.1. Cross-section morphology

The cross-section morphologies of blank PEO, PE-1S and EE-3S, together with the average thickness of epoxy layers in each composite coating are presented in Fig. 2. Without epoxy sealing, the bare PEO layer (Fig. 2(a), thickness 23.4 ± 3.4 μm) reveals a typical cross-section morphology, as disclosed in reference [5, 42]. Two distinctive layers including outer porous layer and inner compact layer can be distinguished from the cross-section. The outer porous layer comprising micropores and defects takes a great majority of the coating volume, whilst the inner layer is much thinner (approx. 1 to 2 μm) but compact. The introduction of pore band between the outer and inner layers can be ascribed to unbalanced growth kinetics of the anodized layer towards electrolyte and metallic substrate, which is closely related with the adoption of experimental parameters (*biz.* electrolyte concentration, power regime and processing time *etc.*) [5]. Because of the existence of the described porous microstructure, a great inhibitor storage capability can be expected for PEO layers. After dipping in epoxy formulation (Fig. 2(b) and 2(c)), uniform top epoxy layers are found upon the sample surface and, in specific, most of the vacant volume in PEO coating is filled up by the epoxy component.

In terms of the thickness of epoxy layers (Fig. 2(d)), EE-3S registers the highest thickness of 16.7 ± 0.3 μm, which is about 1.7 μm thicker than that of PE-3S prepared using the same dip-coating parameters. This difference in thickness suggests the partly consumption of epoxy formulation by penetration into the pores and cracks in the PEO layers. Furthermore, increasing the dipping repetition also contributes to the increase of thickness of epoxy layer: 1.5 μm increase is found when the immersion repetition increases from once (PE-1S: 13.5 ± 1.2 μm) to three times (PE-3S: 15 ± 1.4 μm). On the other hand, the parameter of immersion period imposes negligible impact on epoxy layer thickness. When the immersion period simply increases from 5 s (PE-1S: 13.5 ± 1.2 μm) to 1 min (PE-1S: 13.3 ± 0.9 μm), the reduction in thickness is only 0.2 μm, which is negligible with considering possible errors involved in different experimental steps.

3.2. Electrochemical impedance spectroscopy (EIS)

Electrochemical impedance spectroscopy (EIS) was carried out periodically to evaluate the corrosion properties of all the hybrid coatings in 3.5 wt.% NaCl solution for one month. Fig. 3 shows the Bode plots recorded after 1 h, 1 d, 1 week, 2 weeks and 3 weeks and 4 weeks immersion for the epoxy coated samples

with and without PEO treatment. It can be seen that all the test samples demonstrate a predominantly capacitive response in a wide frequency range. Besides, the initial low frequency (0.01 Hz) impedance value of all the specimens is close to 10^{10} ohm·cm^2, which indicates a high corrosion resistance as a result of the strong barrier properties of epoxy coatings and acceptable sealing of the porous layers, as well visible at respective frequencies and briefly described below.

With time, all the coated systems demonstrate important changes in the impedance spectra. The coating system with fluoride conversion layer initially shows two well-defined relaxation processes. The one at high frequencies can be assigned to the barrier properties of epoxy-polymer layer while the time constant at low frequencies is associated to the response from the fluoride layer. However, the response from the conversion film practically disappears after few days of immersion while the barrier properties of the polymer coating are stable and kept at reasonably high level throughout the full immersion test.

The PE-1S coating prepared with single immersion and short dipping time (5 s) in epoxy formulation has a relaxation process at the beginning of the immersion. At this stage, the coating system responds as one-layer high-barrier coating. However, the situation changes very rapidly during immersion revealing appearance of new time constants and fast decrease of the impedance values especially in the middle to low frequency region. After only 1 day of immersion, the low frequency impedance decreases by one order of magnitude (10^8 ohm·cm^2) in comparison to its initial value. At the same time, at least three time constants can be observed on the impedance spectra. The high frequency one is related to the epoxy-based polymer layer. The relaxation process at middle frequencies can be associated to the response from the PEO layer. The response in the low frequency area is most probably related to the initiation of electrochemical activity at the Mg/PEO interface. It cannot be also excluded that this time constant is related to the dense layer of PEO coating present at the interface rather than to the corrosion. The evolution of these time constants on impedance spectra with immersion time is of particular importance. After initial fast decrease, the barrier properties of the polymer layer demonstrate a relatively slow decay. In contrast, the PEO layers evolve very fast showing an important increase of capacitance and decrease of the pore resistance with time. Such a behavior is most probably related to the fact that during the short single coating application dipping the polymer does not sufficiently penetrate into the PEO pores, which are then filled with electrolyte during the corrosion tests. This effect can lead to an accelerated degradation of the coated substrate.

Simply extending the immersion time in the epoxy formulation from 5 s to 60 s, an improvement in corrosion performance has been achieved by PE-1L (Fig. 3(c)). There is no new time constant appearing at middle frequencies during the immersion in contrast to the previous case. Thus, separation of responses from polymer and outer PEO layer is prevented. The porous PEO sealed with the polymer acts as a single composite barrier layer. No signs of corrosion processes are detected even after 4 weeks of immersion, which confirms the restricted penetration of corrosive species towards Mg substrate and constant protection by the hybrid coating (PE-1L).

Multiple dipping during the coating application also leads to a better pore sealing resulting in a very stable composite coating, which acts as a single layer as indicated by only one time constant during the full immersion period (Fig. 3(d)). The coating keeps very high barrier properties even after one month of immersion in NaCl solution. Adding inhibitor into PEO pores does not deteriorate the barrier properties remarkably, though a slight separation of two relaxation processes can be observed. It can be related to restricting access of polymer formulation into the pores during the dip-coating application after the inhibitor loading process has been performed. PE-3S (Fig. 3(d)) and PE-3S-Inh (Fig. 3(e)) reveal minor deterioration in protective capability throughout EIS measurements. With longer immersion times, the low frequency impedance values of PE-3S keep decreasing slowly, while that for PE-3S-Inh remains almost stable until the end of corrosion test, Fig. 3(e). This result suggests the additional suppression of degradation at the interface by the incorporated inhibitor when corrosion occurs on Mg surface caused by the penetration of corrosive electrolyte through the hybrid coating. By the end of the EIS test, the impedance of the PE-3S and PE-3S-Inh coatings are both stabilized around 10^9 ohm·cm^2, which is ten times higher than that of the EE-3S without PEO layer.

The surface morphology of specimens after one month of EIS measurements was observed using optical microscopy. Fig. 4 presents the obtained images, which are highly consistent with the EIS results shown in Fig. 3. For the reference specimen (EE-3S), a complex filiform corrosion morphology with significantly expanded area even beyond the field exposed to electrolyte can be visually identified. This indicates the penetration of NaCl electrolyte through the epoxy layer resulting in degradation at the interface and corrosion of Mg underneath. In contrast, most hybrid PEO-epoxy coatings exhibit an intact surface at current magnification with an exception of PE-1S. A few corrosion spots (Fig. 4(b)) appear on the surface of PE-1S revealing the localized corrosion failure of the hybrid coating. Through the comparison of the corroded surface morphology between EE-3S and PE-1S, it can be revealed that the spread of corrosion zone is sufficiently impeded by the introduced PEO layers in the hybrid coating system.

Furthermore, SEM and EDS were employed to analyze the morphology and composition of the local corrosion spots on EE-3S and PE-1L coatings, as shown in Fig. 5. The presence of Mg and O elements on top of the epoxy layers (insets in Fig. 5(b) and 5(d)) confirms the penetration of the protective layers by corrosive medium and overflow of corrosion products ($MgO/Mg(OH)_2$). The failure of the epoxy layer is further confirmed by the formation of corrosion products observed from the cross-sectional view of EE-3S sample (inset in Fig. 5(b)). Unlike the EE-3S characterized by uniform degradation morphology, limited number of pitting corrosion dots are shown on the corroded PE-1S coating after monthly immersion. At higher magnification, cluster of island-like spots are covered by a large blister. Such a characteristic indicates the corrosion of Mg substrate initializes from the individual pores of PEO layer after the partially failure of the epoxy layer. The formation of blister can be ascribed to the released hydrogen gas produced as the cathodic reaction products ($2H_2O+2e\rightarrow 2OH^-+H_2$) in the corrosion cell. As processing of corrosion in the

local defective area, the blister would expect to evolve into a larger one but with less decreased corrosion resistance due to the "fault-tolerate" property of the epoxy layer.

3.3. Scanning Vibrating Electrode Technique (SVET)

To reveal the active corrosion protection capability of the hybrid coating system resulted from the incorporated inhibitor (3-MSA), SVET measurements were performed on PE-3S and PE-3S-Inh samples. Artificial defects were intentionally introduced reaching the substrate for simulating the practical conditions, in which damage occurs on the hybrid coatings resulting in partially exposure of Mg substrate to the corrosive electrolyte. The position of introduced defects and their dimensions are illustrated in Fig. 6. The local current density was mapped over the defective area (approx. 4 mm^2) on both samples for 24 hours, as shown in Fig. 7. The first scan (0 h) is carried out immediately after the addition of 0.05 M NaCl solution. For the blank PE-3S without inhibitor, the corrosion attack is initialized within the large linear scratch, and is characterized by high anodic (404.5 $\mu A \cdot cm^{-2}$) and mild cathodic (-79.7 $\mu A \cdot cm^{-2}$) activities. After 6 h of immersion, the anodically active sites shift to the two round defects and much weakened cathodic (-23.4 $\mu A \cdot cm^{-2}$) site is found in the upper defect. This dissipation of the localized corrosion can be explained by the passivation of the Mg with formation of $Mg(OH)_2$ that covers the exposed substrate and provides temporary protection. However, up to 24 h, a significant expansion of electrochemically active area and increase of peak current density are observed. This indicates the failure of the passivation layer and outbreak of general uniform corrosion in the defective areas.

The sample PE-3S-Inh with incorporation of inhibitor (3-MSA) in the PEO layer shows much lower anodic current density (118.8 $\mu A \cdot cm^{-2}$) together with an similar cathodic (-107.5 $\mu A \cdot cm^{-2}$) activity at 0 h scan. This suggests the function of inhibitor as the initialization of corrosion. By 6 h, the initial active zone observed in the linear scratch decreases significantly and the overall active area shrinks into much smaller region confining within the hole-like defects. By the end of measurement (24 h), the area of exposed due to the artificial defects remains virtually inactive comparing to actively corroding reference sample. Hence, through comparison of the results of the samples without and with inhibitor, it can be confirmed that the incorporated inhibitor contributes to impede the corrosion process by suppressing the electrochemical activities (anodic and/or cathodic) within the defective area.

In order to get a clear sense about the evolution of corrosion and evaluate the corrosion kinetics of both samples without and with inhibitor incorporation, the peak anodic and cathodic current density in varied periods is summarized in the format of stacked column. As shown in Fig. 8, the gap (Δ_{cp}) between peak anodic and cathodic current intensity is sustained at 403 $\mu A \cdot cm^{-2}$ (24 h) after the temporary protection by the hydroxide products for the inhibitor-free specimen (PE-3S), whereas a consecutive reduction in this value is revealed for PE-3S-Inh whose final value at 24 h is only about 80 $\mu A \cdot cm^{-2}$. With respect to this difference, much weaker corrosion tendency is expected for the inhibitor incorporating sample PE-3S-Inh.

4. Discussion

4.1. Influence of dipping parameters on the deposition of epoxy layer

As indicated by EIS and corresponding surface analysis results (Fig. 3-5), the deposited epoxy layers act as the first barrier that impedes the penetration of corrosive species into the pores of PEO layers. Comparing to HF conversion and PEO layers, much higher impedance is registered for the epoxy layers. The superior corrosion performance of PE-3S sample can be ascribed to not only the high chemical stability (carbon-carbon and ether bonds) but the sealing effect of epoxy formulation on pores and cracks on the surface of PEO layers. The presence of corrosion defects upon EE-3S indicates the permeable property of the top epoxy layer, which probably caused by the presence of extremely tiny pores within the epoxy layers due to the evaporation of solvent of mixture epoxy formulation during its solidification. In addition, the obviously different corrosion performance among hybrid PEO-epoxy samples (*i.e.* PE-1S, PE-1L and PE-3S) shown in Bode spectra (Fig. 3) also highlights the importance of the parameters applied in the dip-coating process.

The surface morphologies of blank PEO coating before and after epoxy sealing (PE-1S, PE-1L and PE-3S) are presented in Fig. 9. As shown, homogeneous epoxy layers can be found on the top of intermediate anodized layers, even for PE-1S produced by a single fast (5 s) dipping, which agrees well with the cross-sectional morphology in Fig. 3(b). However, incomplete-sealed pores are still detectable upon the surface when observing at higher magnification. The presence of these unsealed pores in epoxy layer can be ascribed to insufficient infiltration of the epoxy formulation into the micro pores in the PEO layers due to the short delay (5 s) in epoxy solution. As follows, evaporation of volatile solvent coupled with shrinkage of the epoxy polymer facilitates the generation of open pores when the samples are cured at designated temperature (150 °C). As a result, the corrosive medium can access the hybrid coating system through these unsealed pores, which subsequently causes corrosion attack of Mg substrate shortly after the degradation of anodized PEO layers. Nevertheless, increasing the immersion period in epoxy formulation to 60 s (PE-1L, Fig. 9(b)) decreases the number of unsealed pores but minor impact (0.1 μm difference) on the thickness of epoxy layer. This phenomenon can be explained by the sufficient penetration or diffusion of epoxy formulation into the pores on PEO layer during a longer immersion in epoxy formulation. Such a strengthen effect of immersion period on the coating is again confirmed in EIS results, in which PE-1L registers a lower degradation rate and one order of magnitude higher expired impedance value than those of PE-1S. On the other hand, trippling the dipping in epoxy formulation brings PE-3S sample thicker (15 μm) but better-sealed epoxy layer, and absence of any visible open pores on the surface at the same magnification as the other samples. Correspondingly, even higher impedance and stable barrier performance are characterized by PE-3S throughout the EIS measurement, which demonstrates the effective sealing of the pores and defects in the anodized layers. Hence, it deducible that increasing the dipping repetition is more effective in producing durable epoxy layer upon porous PEO layers.

4.2. Active protection mechanism

As soon as the occurrence of the mechanical damage of the hybrid coatings, the active protection mechanism caused by the incorporated inhibitor is triggered, as manifested in SVET results in Fig. 7 and 8. Considering the layered microstructure of PEO coatings, the inhibitor molecules are expected to be abundantly stored in different types of pores and pore band specifically, as schematically demonstrated in Fig. 10(a). When the scratched samples are immersed in the corrosive medium, the stored inhibitor molecule dissolves in the electrolyte increasing its concentration at the local defective area. Two plausible inhibition mechanisms, denoted as I and II process in Fig. 10(c), explain the suppression of electrochemical activities in this area, comprising of physical/chemical adsorption and forming complex with detrimental impurities. Attracted by the net charge on the Mg surface, the inhibitor anions (denoted as specifically adsorbed molecule in reference [43]) tend to lose their coordinated water molecule and be absorbed on the bare Mg surface with formation of the inner Helmholtz plane (Fig. 10(c)). Moreover, as suggested in literature [30, 44], electrostatic interactions can be formed between carboxylate polar group and Mg^{2+} whilst the hydrophobic alkyl and hydroxyl ends are inversely located towards the electrolyte repelling the water molecule away from the adsorbed inhibitor layer. On the other hand, the inhibitor molecules can also form complex with detrimental impurities (*e.g.* Fe) avoiding the re-deposition of these detrimental elements on the Mg surface. The systematic explanation about the Fe re-deposition model and formation of inhibitor-Fe complex can be found in literature [40, 45]. Eventually, the localized corrosion is effectively suppressed revealing active protection response against corrosion attack.

5. Conclusion

An active corrosion protective coating system was built on Mg surface. Porous PEO layer was introduced as micro/nano reservoir for storing corrosion inhibitor (sodium salt of 3-methylsalicylate), which was sealed up by a top epoxy layer. Longer period immersion (60 s) favored the penetration of epoxy formulation into the pores and defects in PEO layers, whilst increase in thickness and compactness of epoxy layer were found by tripling the dipping repetition in epoxy formulation. Both strategies contributed to the strengthen of the barrier property of the epoxy layers, which was confirmed by the EIS results. During the degradation process, epoxy polymer served as a strong barrier restricting the penetration of corrosive medium into the hybrid coating system, whilst intermediate PEO layer mainly suppressed the propagation of electrolyte through the pathways and expansion of the corrosion spots. The active protective performance imposed by the incorporated inhibitors is confirmed by the localized characterization technique (SVET) on artificially scratched specimens. The electrochemically active areas (anodic and cathodic) and current density were reduced to a lower level by the incorporated inhibitor after the passivation period of 6 hours. Two plausible inhibition mechanisms were proposed including physical/chemical adsorption and/or formation of complex between detrimental impurities cations and inhibitor molecules.

Funding: This work was supported by the China Scholarship Council [Grant number: 201506120140];

Data availability:

The raw/processed data required to reproduce these findings cannot be shared at this time as the data also forms part of an ongoing study.

Acknowledgement

The technical support of Mr. Volker Heitmann and Mr. Ulrich Burmester during this work is gratefully acknowledged. Junjie Yang thanks China Scholarship Council (Grand No. 201506120140) for the award of fellowship and funding. Dr. S.V. Lamaka acknowledges the financial support of Alexander von Humboldt Foundation via Experienced Researcher Grant. Dr. D. Snihirova acknowledges the financial support of Alexander von Humboldt Foundation via Postdoctoral Researcher Grant. Dr. Xiaopeng Lu acknowledges the financial support of the National Natural Science Foundation of China (NO. U1737102), Young Elite Scientists Sponsorship Program by China Association for Science and Technology (2017QNRC001) and the Fundamental Research Funds for the Central Universities (N170203006).

References:

[1] A.L. Yerokhin, X. Nie, A. Leyland, A. Matthews, S.J. Dowey, Plasma electrolysis for surface engineering, Surface & Coatings Technology, 122 (1999) 73-93.

[2] A. Krzakala, A. Kazek-Kesik, W. Simka, Application of plasma electrolytic oxidation to bioactive surface formation on titanium and its alloys, Rsc Advances, 3 (2013) 19725-19743.

[3] F.C. Walsh, C.T.J. Low, R.J.K. Wood, K.T. Stevens, J. Archer, A.R. Poeton, A. Ryder, Plasma electrolytic oxidation (PEO) for production of anodised coatings on lightweight metal (Al, Mg, Ti) alloys, Transactions of the Institute of Metal Finishing, 87 (2009) 122-135.

[4] C. Blawert, W. Dietzel, E. Ghali, G.L. Song, Anodizing treatments for magnesium alloys and their effecton corrosion resistance in various environments, Advanced Engineering Materials, 8 (2006) 511-533.

[5] R.O. Hussein, X. Nie, D.O. Northwood, An investigation of ceramic coating growth mechanisms in plasma electrolytic oxidation (PEO) processing, Electrochimica Acta, 112 (2013) 111-119.

[6] J. Liang, P.B. Srinivasan, C. Blawert, M. Störmer, W. Dietzel, Electrochemical corrosion behaviour of plasma electrolytic oxidation coatings on AM50 magnesium alloy formed in silicate and phosphate based electrolytes, Electrochimica Acta, 54 (2009) 3842-3850.

[7] R.O. Hussein, D.O. Northwood, X. Nie, The effect of processing parameters and substrate composition on the corrosion resistance of plasma electrolytic oxidation (PEO) coated magnesium alloys, Surface and Coatings Technology, 237 (2013) 357-368.

[8] L. Zhang, J.Q. Zhang, C.F. Chen, Y.H. Gu, Advances in microarc oxidation coated AZ31 Mg alloys for biomedical applications, Corrosion Sci., 91 (2015) 7-28.

[9] P. Bala Srinivasan, J. Liang, R.G. Balajeee, C. Blawert, M. Störmer, W. Dietzel, Effect of pulse frequency on the microstructure, phase composition and corrosion performance of a phosphate-based plasma electrolytic oxidation coated AM50 magnesium alloy, Applied Surface Science, 256 (2010) 3928-3935.

[10] T. Narayanan, M.H. Lee, A simple strategy to modify the porous structure of plasma electrolytic oxidation coatings on magnesium, Rsc Advances, 6 (2016) 16100-16114.

[11] K.M. Lee, B.U. Lee, S.I. Yoon, E.S. Lee, B. Yoo, D.H. Shin, Evaluation of plasma temperature during plasma oxidation processing of AZ91 Mg alloy through analysis of the melting behavior of incorporated particles, Electrochimica Acta, 67 (2012) 6-11.

[12] M. Toorani, M. Aliofkhazraei, M. Golabadi, A.S. Rouhaghdam, Effect of lanthanum nitrate on the microstructure and electrochemical behavior of PEO coatings on AZ31 Mg alloy, Journal of Alloys and Compounds, 719 (2017) 242-255.

[13] X.P. Lu, C. Blawert, K.U. Kainer, M.L. Zheludkevich, Investigation of the formation mechanisms of plasma electrolytic oxidation coatings on Mg alloy AM50 using particles, Electrochim. Acta, 196 (2016) 680-691.

[14] M. Mohedano, C. Blawert, M.L. Zheludkevich, Cerium-based sealing of PEO coated AM50 magnesium alloy, Surface and Coatings Technology, 269 (2015) 145-154.

[15] Z.J. Li, Y. Yuan, X.Y. Jing, Composite coatings prepared by combined plasma electrolytic oxidation and chemical conversion routes on magnesium-lithium alloy, Journal of Alloys and Compounds, 706 (2017) 419-429.

[16] Z.J. Li, Y. Yuan, Preparation and characterization of superhydrophobic composite coatings on a magnesium-lithium alloy, Rsc Advances, 6 (2016) 90587-90596.

[17] S.V. Gnedenkov, S.L. Sinebryukhov, D.V. Mashtalyar, I.M. Imshinetskiy, Composite fluoropolymer coatings on Mg alloys formed by plasma electrolytic oxidation in combination with electrophoretic deposition, Surface & Coatings Technology, 283 (2015) 347-352.

[18] Y.K. Kim, Y.S. Jang, Y.H. Lee, H.K. Yi, T.S. Bae, M.H. Lee, Effect of Ca-P compound formed by hydrothermal treatment on biodegradation and biocompatibility of Mg-3Al-1Zn-1.5Ca alloy; in vitro and in vivo evaluation, Scientific Reports, 7 (2017).

[19] M. Sun, A. Yerokhin, A. Matthews, M. Thomas, A. Laukart, M. von Hausen, C.P. Klages, Characterisation and Electrochemical Evaluation of Plasma Electrolytic Oxidation Coatings on Magnesium with Plasma Enhanced Chemical Vapour Deposition Post-Treatments, Plasma Process. Polym., 13 (2016) 266-278.

[20] D. Ivanou, K. Yasakau, S. Kallip, A. Lisenkov, M. Starykevich, S. Lamaka, M. Ferreira, M. Zheludkevich, Active corrosion protection coating for a ZE41 magnesium alloy created by combining PEO and sol–gel techniques, RSC Advances, 6 (2016) 12553-12560.

[21] D.K. Ivanou, M. Starykevich, A.D. Lisenkov, M.L. Zheludkevich, H.B. Xue, S.V. Lamaka, M.G.S. Ferreira, Plasma anodized ZE41 magnesium alloy sealed with hybrid epoxy-silane coating, Corrosion Sci., 73 (2013) 300-308.

[22] F. Brusciotti, D.V. Snihirova, H. Xue, M.F. Montemor, S.V. Lamaka, M.G.S. Ferreira, Hybrid epoxy–silane coatings for improved corrosion protection of Mg alloy, Corrosion Sci., 67 (2013) 82-90.

[23] R.-G. Hu, S. Zhang, J.-F. Bu, C.-J. Lin, G.-L. Song, Recent progress in corrosion protection of magnesium alloys by organic coatings, Progress in Organic Coatings, 73 (2012) 129-141.

[24] W.B. Yang, Q.B. Li, Q. Xiao, J. Liang, Improvement of corrosion protective performance of organic coating on low carbon steel by PEO pretreatment, Progress in Organic Coatings, 89 (2015) 260-266.

[25] S.V. Lamaka, H.S. Xue, N. Meis, A.C.C. Esteves, M.G.S. Ferreira, Fault-tolerant hybrid epoxy-silane coating for corrosion protection of magnesium alloy AZ31, Progress in Organic Coatings, 80 (2015) 98-105.

[26] S.V. Lamaka, G. Knornschild, D.V. Snihirova, M.G. Taryba, M.L. Zheludkevich, M.G.S. Ferreira, Complex anticorrosion coating for ZK30 magnesium alloy, Electrochimica Acta, 55 (2009) 131-141.

[27] N.V. Phuong, B.R. Fazal, S. Moon, Cerium-and phosphate-based sealing treatments of PEO coated AZ31. Mg alloy, Surface & Coatings Technology, 309 (2017) 86-95.

[28] S.V. Lamaka, B. Vaghefinazari, D. Mei, R.P. Petrauskas, D. Höche, M.L. Zheludkevich, Comprehensive screening of Mg corrosion inhibitors, Corrosion Sci., 128 (2017) 224-240.

[29] I.A. Kartsonakis, S.G. Stanciu, A.A. Matei, E.K. Karaxi, R. Hristu, A. Karantonis, C.A. Charitidis, Evaluation of the protective ability of typical corrosion inhibitors for magnesium alloys towards the Mg ZK30 variant, Corrosion Sci., 100 (2015) 194-208.

[30] N. Dinodi, A.N. Shetty, Alkyl carboxylates as efficient and green inhibitors of magnesium alloy ZE41 corrosion in aqueous salt solution, Corrosion Sci., 85 (2014) 411-427.

[31] J. Hu, D. Huang, G. Zhang, G.-L. Song, X. Guo, Research on the inhibition mechanism of tetraphenylporphyrin on AZ91D magnesium alloy, Corrosion Sci., 63 (2012) 367-378.

[32] A. Frignani, V. Grassi, F. Zanotto, F. Zucchi, Inhibition of AZ31 Mg alloy corrosion by anionic surfactants, Corrosion Sci., 63 (2012) 29-39.

[33] D. Huang, J. Hu, G.-L. Song, X. Guo, Inhibition effect of inorganic and organic inhibitors on the corrosion of Mg–10Gd–3Y–0.5Zr alloy in an ethylene glycol solution at ambient and elevated temperatures, Electrochimica Acta, 56 (2011) 10166-10178.

[34] N.H. Helal, W.A. Badawy, Environmentally safe corrosion inhibition of Mg–Al–Zn alloy in chloride free neutral solutions by amino acids, Electrochimica Acta, 56 (2011) 6581-6587.

[35] H. Gao, Q. Li, F.N. Chen, Y. Dai, F. Luo, L.Q. Li, Study of the corrosion inhibition effect of sodium silicate on AZ91D magnesium alloy, Corrosion Sci., 53 (2011) 1401-1407.

[36] H. Gao, Q. Li, Y. Dai, F. Luo, H.X. Zhang, High efficiency corrosion inhibitor 8-hydroxyquinoline and its synergistic effect with sodium dodecylbenzenesulphonate on AZ91D magnesium alloy, Corrosion Sci., 52 (2010) 1603-1609.

[37] M.F. Montemor, M.G.S. Ferreira, Analytical characterisation and corrosion behaviour of bis-aminosilane coatings modified with carbon nanotubes activated with rare-earth salts applied on AZ31 Magnesium alloy, Surface and Coatings Technology, 202 (2008) 4766-4774.

[38] A.S. Gnedenkov, S.L. Sinebryukhov, D.V. Mashtalyar, S.V. Gnedenkov, Protective properties of inhibitor-containing composite coatings on a Mg alloy, Corrosion Sci., 102 (2016) 348-354.

[39] A.S. Gnedenkov, S.L. Sinebryukhov, D.V. Mashtalyar, S.V. Gnedenkov, Localized corrosion of the Mg alloys with inhibitor-containing coatings: SVET and SIET studies, Corrosion Sci., 102 (2016) 269-278.

[40] S.V. Lamaka, D. Höche, R.P. Petrauskas, C. Blawert, M.L. Zheludkevich, A new concept for corrosion inhibition of magnesium: Suppression of iron re-deposition, Electrochemistry Communications, 62 (2016) 5-8.

[41] H.Y. Su, W.J. Li, C.S. Lin, Effect of Acid Pickling Pretreatment on the Properties of Cerium Conversion Coating on AZ31 Magnesium Alloy, Journal of the Electrochemical Society, 159 (2012) C219-C225.

[42] X.P. Lu, S.P. Sah, N. Scharnagl, M. Stormer, M. Starykevich, M. Mohedano, C. Blawert, M.L. Zheludkevich, K.U. Kainer, Degradation behavior of PEO coating on AM50 magnesium alloy produced from electrolytes with clay particle addition, Surface & Coatings Technology, 269 (2015) 155-169.
[43] A.J. Bard, L.R. Faulkner, J. Leddy, C.G. Zoski, Electrochemical methods: fundamentals and applications, wiley New York, 1980.
[44] A. Mesbah, C. Juers, F. Lacouture, S. Mathieu, E. Rocca, M. François, J. Steinmetz, Inhibitors for magnesium corrosion: Metal organic frameworks, Solid State Sciences, 9 (2007) 322-328.
[45] D. Hoche, C. Blawert, S.V. Lamaka, N. Scharnagl, C. Mendis, M.L. Zheludkevich, The effect of iron re-deposition on the corrosion of impurity-containing magnesium, Phys. Chem. Chem. Phys., 18 (2016) 1279-1291.

7. Figure captions

Fig. 1 UV spectra of standard (5×10^{-4}, 5×10^{-5} and 5×10^{-6} M) 3-MSA solutions and liquid samples obtained from soaking inhibitor-loaded PEO specimen with 5 min supersonic treatment

Fig. 2 Cross-section SEM images and epoxy layer thickness of hybrid coatings
(a) Blank PEO, (b) PE-1S, (c) EE-3S and (d) average thickness of epoxy layer of hybrid coatings.

Fig. 3 Bode spectra of hybrid coatings immersed in 3.5 wt.% NaCl solution for monthly EIS measurements
(a) EE-3S, (b) PE-1S, (c) PE-1L, (d) PE-3S and (e) PE-3S-Inh.

Fig. 4 Optical microscopy images of specimens after monthly EIS measurements
(a) EE-3S, (b) PE-1S, (c) PE-1L, (d) PE-3S and (e) PE-3S-Inh.

Fig. 5 SEM/EDS analysis of corroded area after monthly EIS measurements
(a-b) EE-3S and (c-d) PE-1S

Fig. 6 Optical microscopy image of artificial defects on hybrid PEO-epoxy specimens introduced for SVET measurements

Fig. 7 SVET contour plots of scratched PEO-epoxy coatings without and with corrosion inhibitor, 3-MSA, incorporated in PEO layer in 0.05 M NaCl solution (a) PE-3S-0h, (b) PE-3S-6h, (c) PE-3S-24h, (d) PE-3S-Inh-0h, (e) PE-3S-Inh-6h and (f) PE-3S-Inh-24h

Fig. 8 Peak current density (anodic and cathodic) on scratched PE-3S without and with inhibitor (3-methylsalicylate) during 24 h immersion in 0.05 M NaCl solution

Fig. 9 SEM images of bare PEO layer without and with epoxy sealing
(a) bare PEO and PE-1S and (b) PE-1L and PE-3S

Fig. 10 Schematic illustration of inhibition mechanism of inhibitor (sodium salt of 3-methylsalicylate)
(a) Intact PE-3S-Inh coating (Cross-section morphology), (b) Occurrence of corrosion on the PE-3S-Inh coating and (c) Two plausible active protection mechanisms for incorporated inhibitor: (I) Physical/chemical adsorption and (II) Formation of Impurity-Inhibitor complex

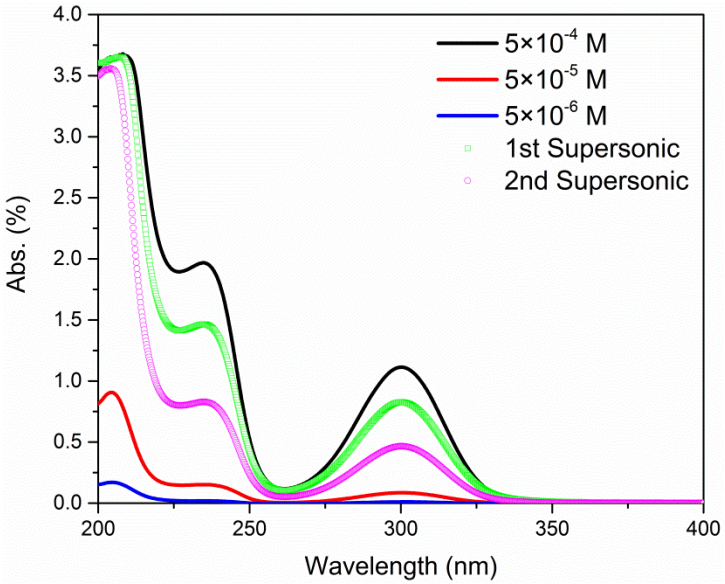

Fig. 1

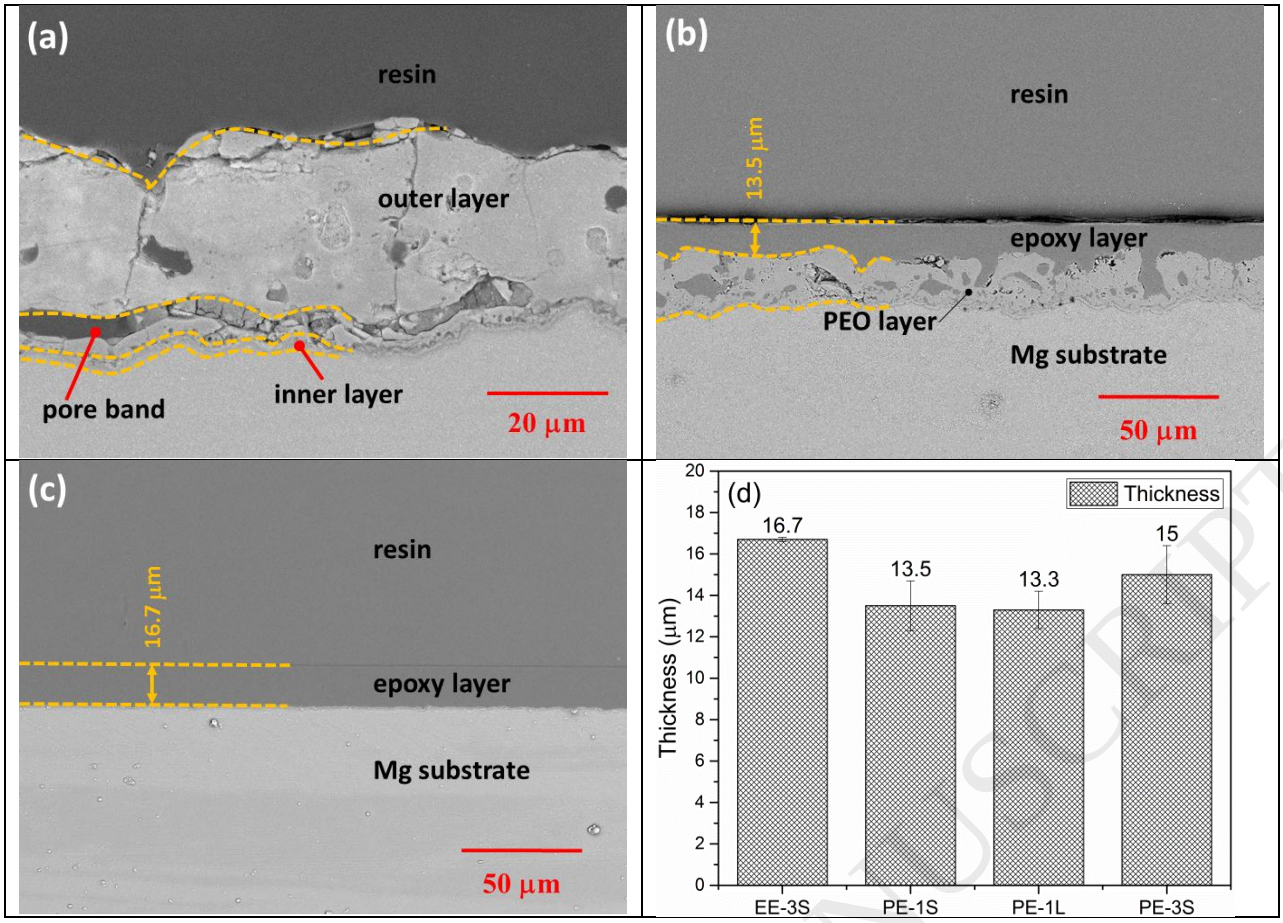

Fig. 2

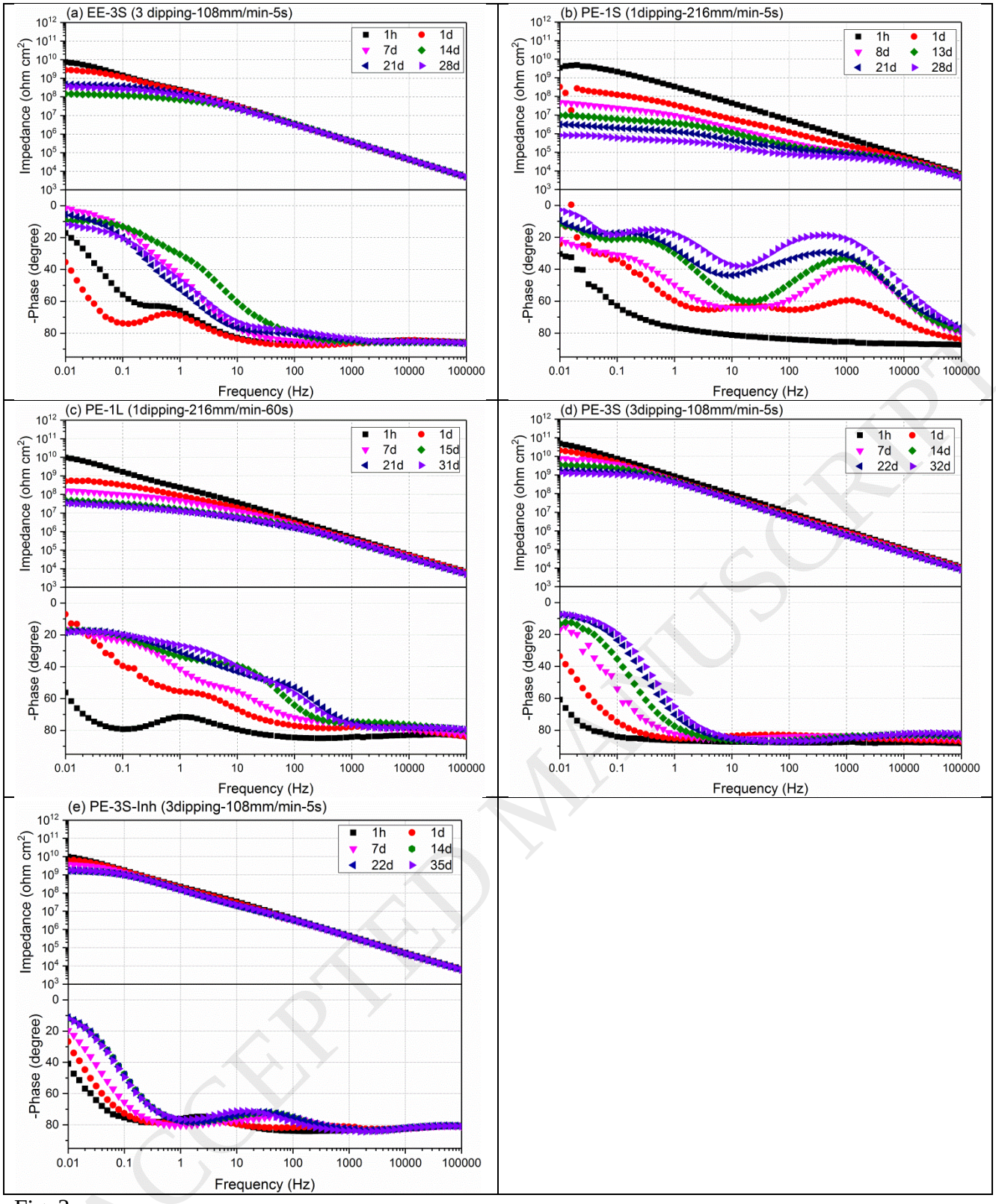

Fig. 3

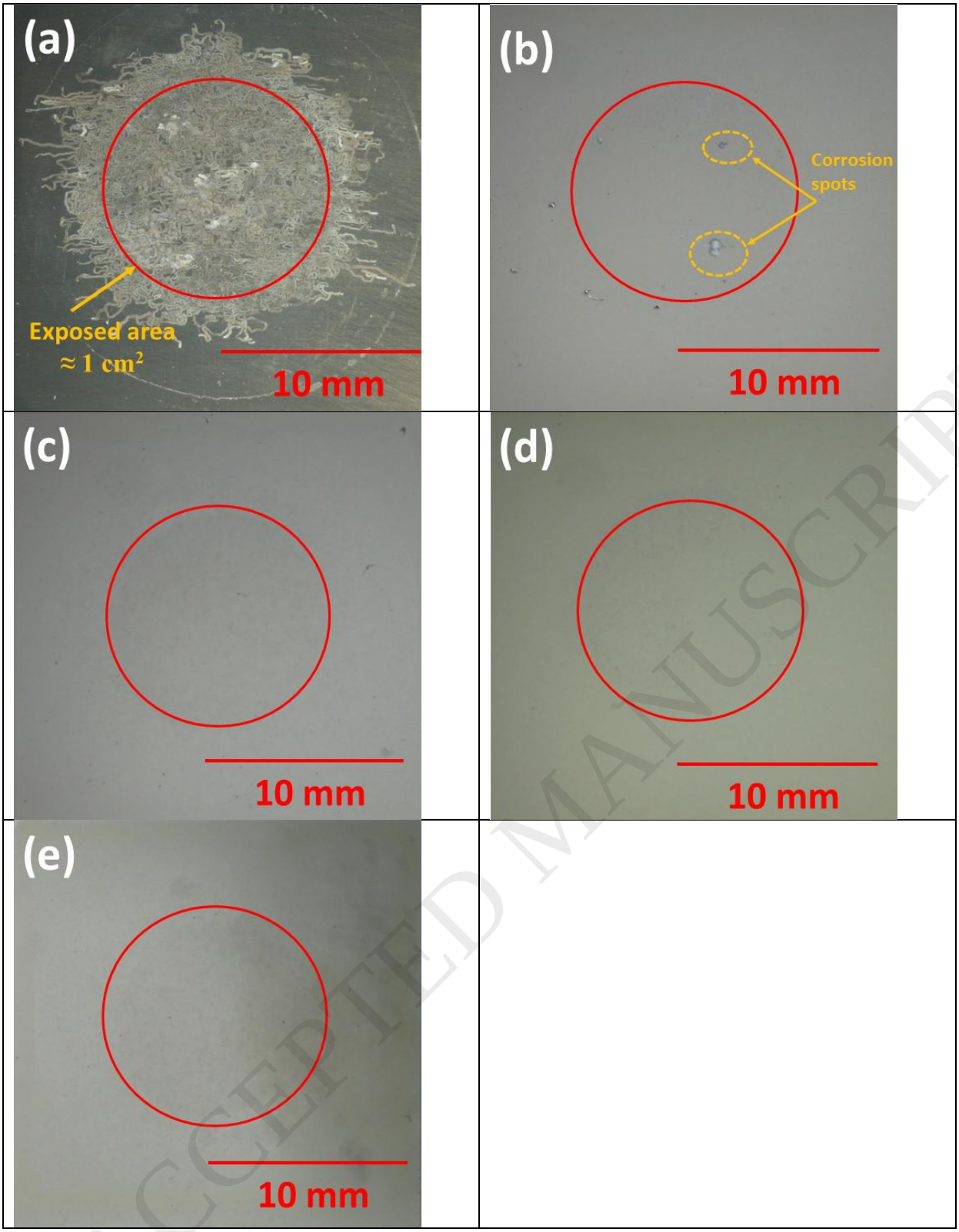

Fig. 4

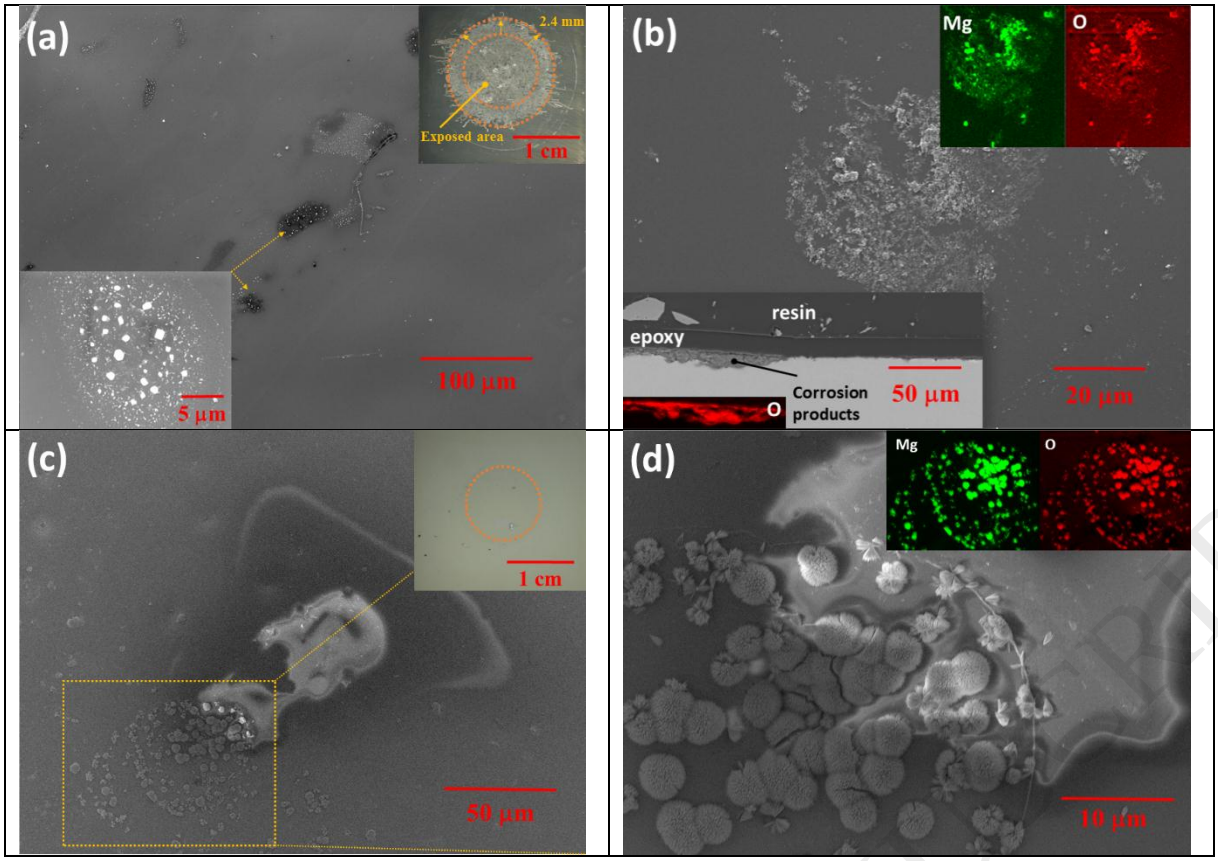

Fig. 5

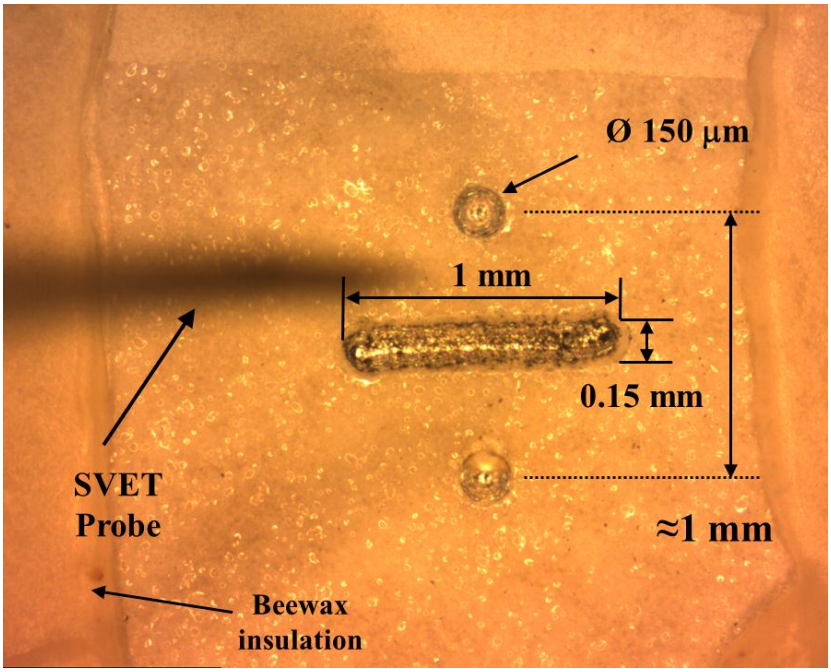

Fig. 6

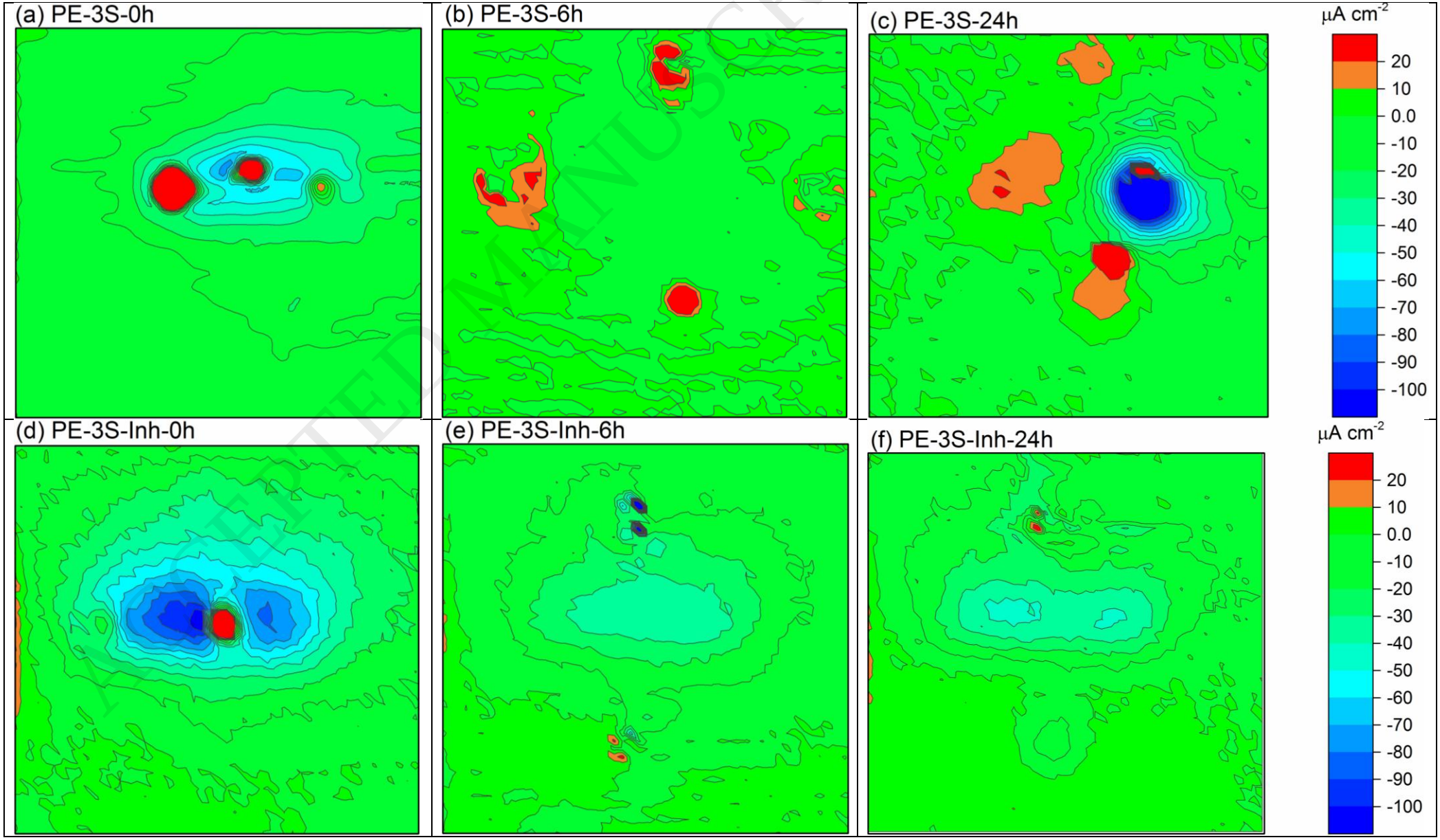

Fig. 7

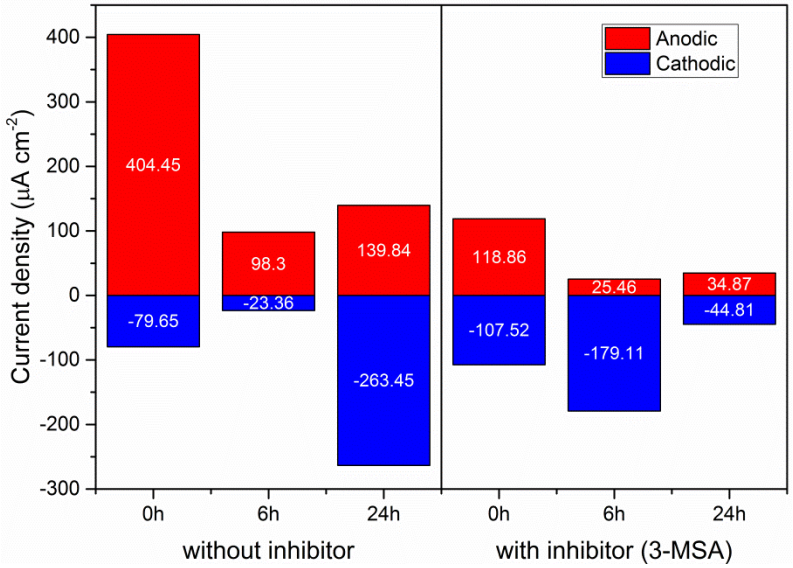

Fig. 8

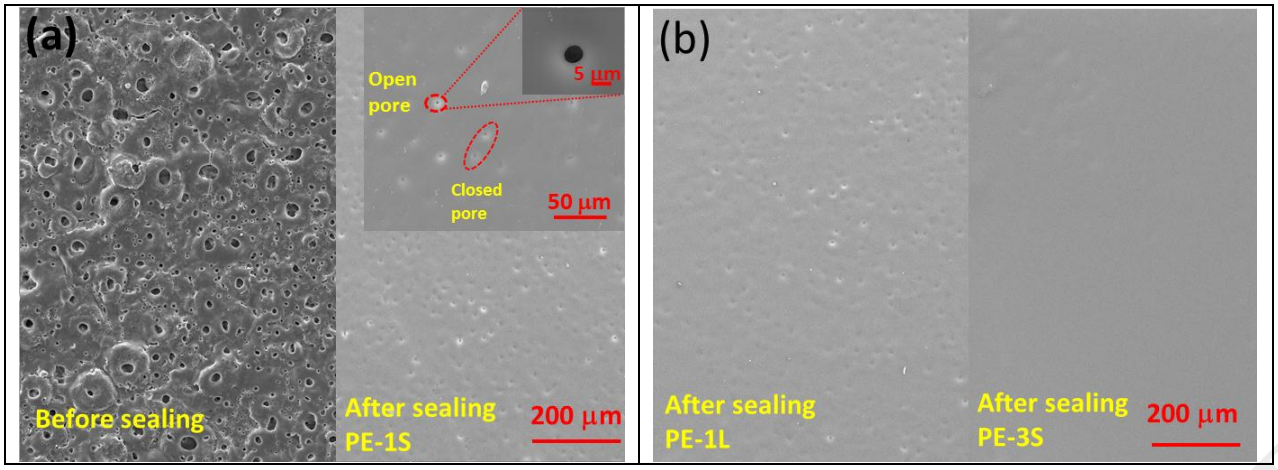

Fig. 9

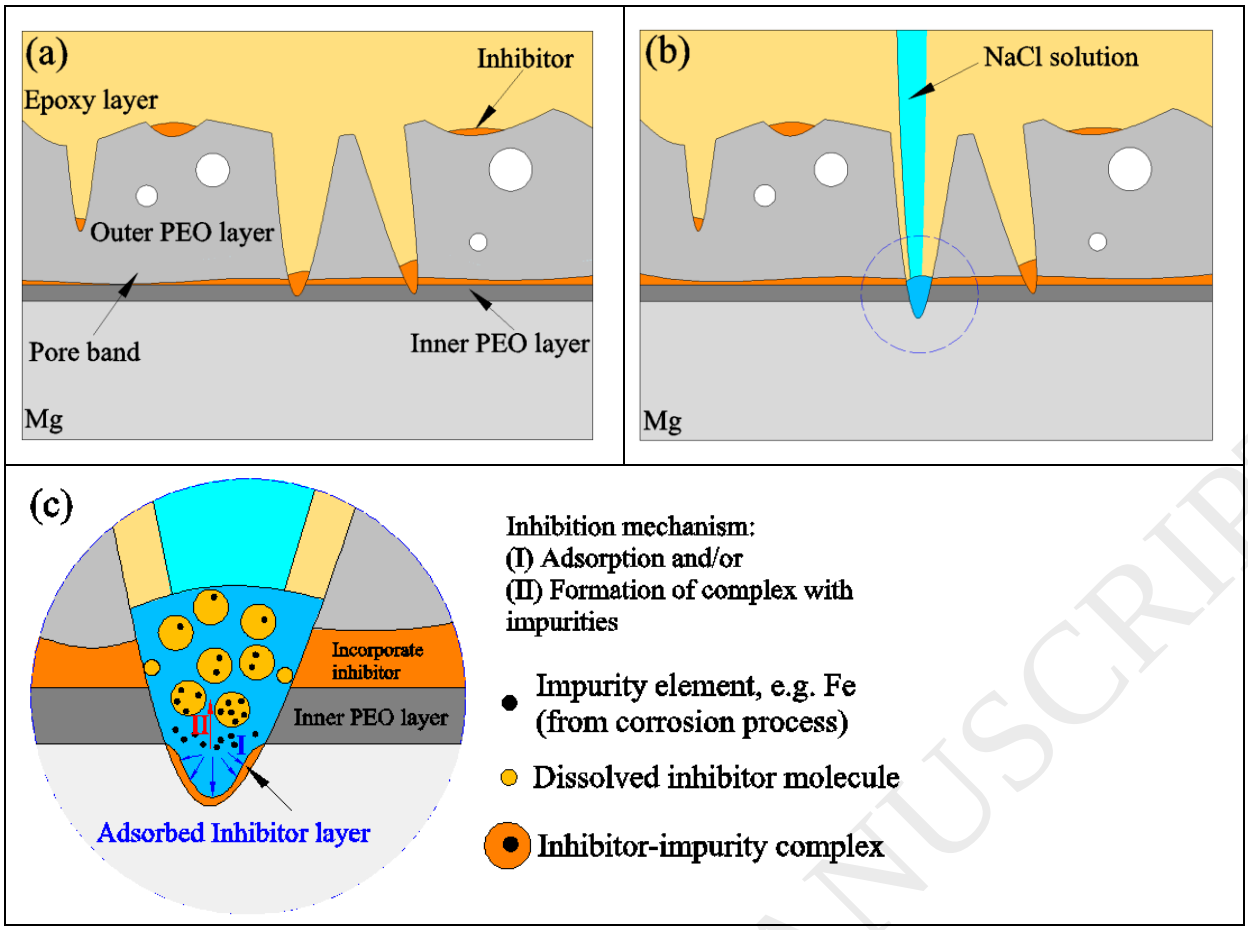

Fig. 10

Table 1 Chemical composition of Mg substrate (wt.%)

Ag	Al	Ca	Cu	Fe	Mn	Ni	Si	Zn	Mg
<0.00005	0.0129	0.0033	0.0004	0.0054	0.02	<0.0002	0.02	0.0018	balance

Table 2 Denomination of samples and parameters involved in the dip-coating process

Denomination	Pre-treatment	Dipping parameters		
		Immersion and withdrawal speed (mm/min)	Immersion repetition (times)	Immersion period (s)
EE-3S	HF etched	108	3	5
PE-1S	PEO	216	1	5
PE-1L	PEO	216	1	60
PE-3S	PEO	108	3	5
PE-3S-Inh	PEO (3-MSA)	108	3	5

Table 3 OCP values in prior to EIS measurements for epoxy coated samples in absence and presence of PEO layers (V vs. Ag/AgCl)

	EE-3S	PE-1S	PE-1L	PE-3S	PE-3S-Inh
1h	-1.90	-1.75	-1.75	-1.37	-1.49
24h	-1.83	-1.75	-1.74	-1.05	-1.53
48h	-1.64	-1.81	-1.81	-1.05	-1.55
168h	-1.60	-1.54	-1.54	-1.36	-1.49